Theoretical and Applied Mechanics Letters 5 (2015) 54–57

Contents lists available at ScienceDirect

Theoretical and Applied Mechanics Letters

journal homepage: www.elsevier.com/locate/taml

Letter

Thrust producing mechanisms in ray-inspired underwater vehicle propulsion

Geng Liu, Yan Ren, Jianzhong Zhu, Hilary Bart-Smith, Haibo Dong *

Department of Mechanical and Aerospace Engineering, University of Virginia, Charlottesville, VA 22904, USA

ARTICLE INFO

Article history:
Received 24 November 2014
Accepted 26 November 2014
Available online 6 January 2015
*This article belongs to the Fluid Mechanics

Keywords:
Hydrodynamics
Bio-inspired autonomous underwater vehicle
Computational fluid dynamics
Vortex dynamics

ABSTRACT

This paper describes a computational study of the hydrodynamics of a ray-inspired underwater vehicle conducted concurrently with experimental measurements. High-resolution stereo-videos of the vehicle's fin motions during steady swimming are obtained and used as a foundation for developing a high fidelity geometrical model of the oscillatory fin. A Cartesian grid based immersed boundary solver is used to examine the flow fields produced due to these complex artificial pectoral fin kinematics. Simulations are carried out at a smaller Reynolds number in order to examine the hydrodynamic performance and understand the resultant wake topology. Results show that the vehicle's fins experience large spanwise inflexion of the distal part as well as moderate chordwise pitching during the oscillatory motion. Most thrust force is generated by the distal part of the fin, and it is highly correlated with the spanwise inflexion. Two sets of inter-connected vortex rings are observed in the wake right behind each fin. Those vortex rings induce strong backward flow jets which are mainly responsible for the fin thrust generation.

A bio-inspired autonomous underwater vehicle (AUV) has been designed as a scientific platform to understand the superior swimming characteristics of batoid fish. Batoid fish such as manta rays (Manta birostris) and cownose rays (Rhinoptera bonasus) are notable for their fast, efficient swimming and high maneuverability. These swimming capabilities arise from flapping of the dorsally flattened pectoral fins, which are also used as control surfaces for depth control and maneuvering. Recent observations in animal propulsion suggest that high efficiency in animal locomotion can be attributed to the stiffness characteristics at the fin tip [1]. In rays' swimming, the large bending of the distal part of the pectoral fin can allow them to actively resist hydrodynamic bending forces while producing propulsion forces. To assess this contribution, the current effort is specifically focused on understanding the hydrodynamics of a ray-inspired underwater vehicle – the MantaBot – where biology is the basis for the design.

The MantaBot consists of two parts: a rigid body rendered from a computer tomography scanning image of a cownose ray and a pair of soft fins driven by tensegrity-based actuators [2] (Fig. 1(a)). The soft fins of this vehicle are highly flexible, have complex planforms, and undergo an oscillatory motion. Specific to this vehicle's body length ($L \sim 43$ cm) and free-swimming velocity ($0.35\ \mathrm{m\cdot s^{-1}}$), the Reynolds number ($Re = UL/\nu$) is approximately 1.5×10^5. At this Reynolds number, the attached flow over the body is most likely laminar but transition to turbulence is expected to occur rapidly in the downstream of MantaBot fins. The flow over the fins can be characterized in terms of a Stokes frequency parameter ($S = \omega Ac/\nu$) where ω, A and c are the fin angular frequency, amplitude and length of the mid-chord, respectively. Typical fin beat frequency of about 2 Hz and fin amplitude and size of about 5 cm and 6 cm, respectively, give $S \approx 3.5 \times 10^4$, which is again in the range where transition from laminar attached flow to turbulence will occur quickly.

Figure 1(a) shows the MantaBot body with kinematic markers (red dots) drawn on its fins, which are used for tracking and performing 3D surface reconstruction later in the process and a schematic of the experimental setup. To measure the fin kinematics of MantaBot in steady swimming, the vehicle is placed in a 5 m long, 1.5 m wide, and 0.6 m deep water tank. Its locomotion is restricted to one degree of freedom (forward translation) using a steel bar, which is connected to a low-friction ball bearing slider on a linear rail.

The MantaBot swimming motion is then recorded by three well calibrated and synchronized video cameras (rear, side, and top) that are operated at 60 Hz with 512×512 pixel resolutions. These cameras are aligned orthogonal to each other and positioned about 0.75 m away from the Mantabot, giving a depth of field of 3–4 body lengths in all directions. The cameras are triggered by a flashing

* Corresponding author.
E-mail address: haibo.dong@virginia.edu (H. Dong).

http://dx.doi.org/10.1016/j.taml.2014.12.004

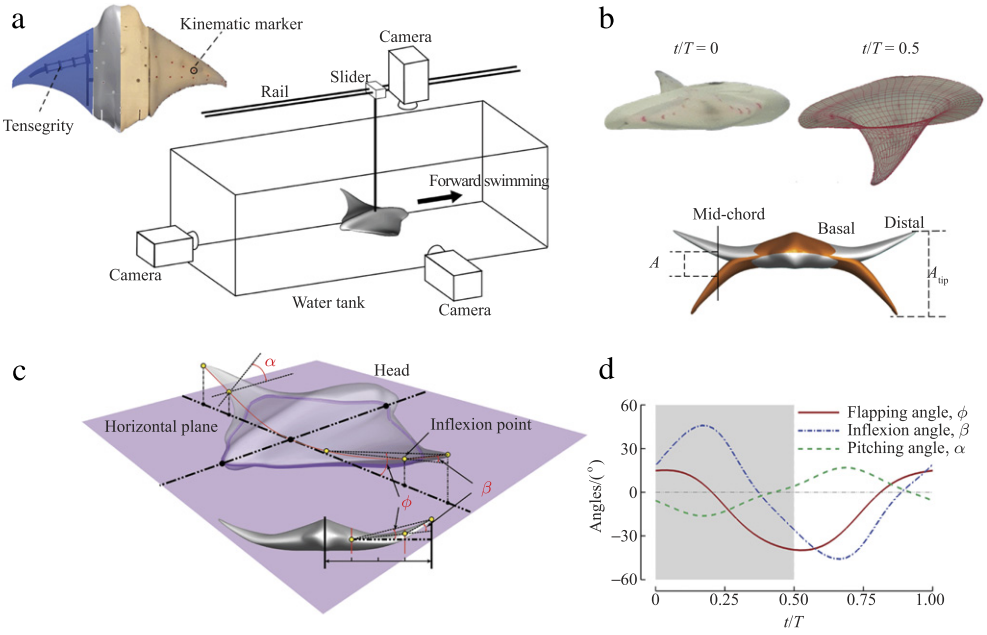

Fig. 1. (a) MantaBot with tensegrity actuator and kinematic markers and experimental measurement setup. (b) Side views of original MantaBot (upper left) and meshed model (upper right) and a front view of the MantaBot model (lower) at $t/T = 0$ and $t/T = 0.5$. (c) Definition for flapping, inflexion and pitching angles (ϕ, β and α, respectively). (d) The time course of the measured kinematics in one typical flapping cycle.

Table 1
Key quantities of the body shape and swimming motion.

L/m	l/m	U/m · s^{-1}	A/m	f/Hz	St	Re
0.428	0.274	0.347	0.05	1.82	0.27	1.5×10^5

light system to minimize the recording delay of each camera. When the MantaBot is in the optimum range, this camera system is able to collect data that is consistently in focus. Usable segments of videos from all sides are identified for kinematics reconstruction based on the quality of images. Among all three cameras, the camera set at the rear is for recording the fin flapping motion and spanwise bending. The videos from this camera are used to measure both the flapping angles and inflexion angles shown in Fig. 1(c). The side camera, along with the top camera, is used to track the motions of all kinematic markers in Fig. 1(a). They are used to accurately measure the chordwise flexibility including the mid-chord pitching angles in Fig. 1(c).

Once these videos are identified, a marker-based 3D surface reconstruction method [3] will then be used to obtain the instantaneous control surfaces of the flapping MantaBot during the steady swimming. These reconstructed 3D surfaces will be meshed using triangular grids and used as inputs for later computational fluid dynamics (CFD) simulations. Details about this method can be found in Ref. [3].

A number of combinations of driving frequency and amplitude of the MantaBot were tested, and the case that achieved the maximum speed was selected for this study. Key quantities of the body shape and locomotion are summarized in Table 1, where L is the body length, l is the fin span length, U is the swimming speed, A is the flapping amplitude of the fin mid-chord, f is the flapping frequency, St is the Strouhal number defined as $St = fA/U$, and Re is the Reynolds number.

The reconstruction model is shown in Fig. 1(b). Upper two plots are the side view of the original MantaBot and the meshed model in 3D reconstruction at the beginning of downstroke and upstroke, respectively. The lower plot is the front view of the model showing the maximum fin bending. The most apparent feature from the fin kinematic reconstruction is the spanwise flapping with large bending at distal part. As shown in Fig. 1(c), the flapping angle ϕ is the angle between the base-to-tip line and the horizontal plane, where the fin base is $0.33l$ away from middle section of the body. The spanwise bending can be quantified by inflexion angle (β) [1]. The maximum bending happens mostly at $0.67l$ from the fin base. This location is defined as the inflexion point shown in Fig. 1(c). β is the angle between the lines of base-to-inflexion point and inflexion point-to-tip. The pitching angle α in Fig. 1(c) is defined as the angle between the chord at inflexion point and the horizontal plane.

Figure 1(d) shows the time course of ϕ, β, and α, which are averaged over four consecutive flapping strokes from meshed fin models. The time variation of ϕ indicates that the basic fin flapping motion is not symmetric. The downward excursion is more than twice the upward excursion. Spanwise bending is prominent because the inflexion angle β has larger peak-to-peak amplitude values among all three angles. The maximum amplitude of β is about 45°, which is slightly larger than the average inflexion angle observed in most swimming and flying animals [1]. This indicates that the MantaBot fins can achieve large amplitude of bending of the distal parts. The chordwise pitching is observed varying in between $\pm 16°$ during this steady swimming motion. It is worth noting that the tensegrity actuation structures in the MantaBot cannot generate chordwise pitching directly. The fin pitching is passively generated by the interaction between the surrounding flows and the soft fins. It is also found that this pitching motion can only be clearly observed in the distal part of the fin.

The hydrodynamic mechanism of the ray-inspired underwater vehicle propulsion is then explored using an immersed boundary method [4] based high fidelity CFD simulation. In particular, the solver is time-accurate and non-dissipative, and allows body motion. The details of the solver can be found elsewhere [5–7]. To study the long-term hydrodynamic performance of the flapping fins in steady swimming, a uniform flow of speed U passing the MantaBot model is utilized to save on computation cost. The goal of current simulations is to capture the key features of the wake structures for addressing the fundamental hydrodynamic mechanisms of the flapping swimming. To this end, the actual Reynolds number is reduced to 1200 for meeting the requirement of the mesh resolution and computation cost by direct numerical simulation of swimming objects [8–12]. This is equivalent to either a smaller size body